A novel intermembrane space–targeting signal docks cysteines onto Mia40 during mitochondrial oxidative folding

Dionisia P. Sideris,[1,2] Nikos Petrakis,[1,3] Nitsa Katrakili,[1] Despina Mikropoulou,[1,2] Angelo Gallo,[5,6] Simone Ciofi-Baffoni,[5,6] Lucia Banci,[5,6] Ivano Bertini,[5,6] and Kostas Tokatlidis[1,4]

[1]Institute of Molecular Biology and Biotechnology, Foundation for Research and Technology Hellas, 70013 Heraklion, Crete, Greece
[2]Department of Biology, [3]Department of Chemistry, and [4]Department of Materials Science and Technology, University of Crete, 71003 Heraklion, Crete, Greece
[5]Magnetic Resonance Center and [6]Department of Chemistry, University of Florence, 50019 Sesto Fiorentino, Florence, Italy

Mia40 imports Cys-containing proteins into the mitochondrial intermembrane space (IMS) by ensuring their Cys-dependent oxidative folding. In this study, we show that the specific Cys of the substrate involved in docking with Mia40 is substrate dependent, the process being guided by an IMS-targeting signal (ITS) present in Mia40 substrates. The ITS is a 9-aa internal peptide that (a) is upstream or downstream of the docking Cys, (b) is sufficient for crossing the outer membrane and for targeting nonmitochondrial proteins, (c) forms an amphipathic helix with crucial hydrophobic residues on the side of the docking Cys and dispensable charged residues on the other side, and (d) fits complementary to the substrate cleft of Mia40 via hydrophobic interactions of micromolar affinity. We rationalize the dual function of Mia40 as a receptor and an oxidase in a two step–specific mechanism: an ITS-guided sliding step orients the substrate noncovalently, followed by docking of the substrate Cys now juxtaposed to pair with the Mia40 active Cys.

Introduction

Cys-containing proteins of the mitochondrial intermembrane space (IMS) are oxidatively folded by Mia40 through the formation of transient mixed disulfides (Chacinska et al., 2004; Naoé et al., 2004; Mesecke et al., 2005; Rissler et al., 2005; Terziyska et al., 2005, 2007; Gabriel et al., 2007; Hell, 2008; Müller et al., 2008; Reddehase et al., 2009). Mia40 also functions as a receptor recognizing these substrates by an unknown mechanism. Current evidence supports a site-specific recognition of the substrate-docking Cys. For example, small Tims dock to Mia40 via their N-terminal end Cys, which pairs with the C-terminal end Cys in an outer disulfide bridge in the folded state (Milenkovic et al., 2007; Sideris and Tokatlidis, 2007). In contrast, Mia40 oxidizes the inner disulfide pair of COX17, surprisingly and unlike the small Tims (Banci et al., 2009). The exact Cox17 Cys used for docking is still unknown. The recent Mia40 solution structure uncovered a hydrophobic cleft that sits adjacent to the active site CPC motif and was proposed to be the substrate-binding domain. Evidence for this proposal relied on mutagenesis of Mia40 residues in this cleft found to be lethal in vivo and decreased substrate binding in vitro (Banci et al., 2009). However, it is still unknown which segments target the substrate to Mia40 to allow correct covalent pairing.

In this study, we describe the signal for targeting different classes of substrates to Mia40 (IMS-targeting signal [ITS]). A similar signal to the ITS was reported by Milenkovic et al. (2009) only for the small Tims and termed mitochondria IMS-sorting signal (MISS). Our data suggest a partial overlap between the ITS and MISS sequences and reveal additional roles for the ITS not reported before. To avoid confusion, we refer to this signal as MISS/ITS.

The MISS/ITS is a peptide of nine residues found in essentially all Mia40 substrates and primes one Cys for docking

Correspondence to Kostas Tokatlidis: tokatlid@imbb.forth.gr

Abbreviations used in this paper: β-Me, β-mercaptoethanol; BN, blue native; cyb2, cytochrome b_2; DHFR, dihydrofolate reductase; GAL, galactose; IMS, intermembrane space; ITC, isothermal titration calorimetry; ITS, IMS-targeting signal; MISS, mitochondria IMS-sorting signal; NTA, nitrilotriacetic acid; OM, outer membrane.

The Rockefeller University Press $30.00
J. Cell Biol. Vol. 187 No. 7 1007–1022
www.jcb.org/cgi/doi/10.1083/jcb.200905134

with the Mia40 active site CPC motif (Banci et al., 2009; Terziyska et al., 2009). The MISS/ITS is necessary and sufficient for IMS targeting to Mia40. Deleting it results in complete loss of import, whereas fusing it to a nonmitochondrial protein targets it to the organelle. The ITS contains enough information for translocation across the outer membrane (OM) independently of Mia40, thus experimentally uncoupling these two processes. One crucial feature of MISS/ITS is that it forms a helix with vital aromatic and hydrophobic residues to the same side of the docking Cys. Hydrophobic noncovalent interactions of this side of the MISS/ITS helix with aliphatic side chains of the Mia40-binding cleft orient the substrate onto Mia40 (sliding step), thus committing the crucial Cys for subsequent covalent disulfide bonding with Mia40 (docking step). This two-step mechanism solves the conundrum of how substrates with no sequence similarity are recognized by Mia40 and explains how they are positioned structurally so that specific cysteines in each substrate bond with the Mia40 active site Cys. Finally, we measured by calorimetry, for the first time, the affinity involved in the crucial noncovalent interactions that guide the substrate onto Mia40 via MISS/ITS.

Results

Cox17 docks onto Mia40 with a different Cys specificity from the small Tims

Mia40 binding to the small Tims strictly depends on their N-terminal end Cys of the twin CX3C motif (Milenkovic et al., 2007; Sideris and Tokatlidis, 2007), but it is unknown whether this is true for Tim-unrelated proteins like Cox17, which contains twin CX9C motifs (Arnesano et al., 2005; Banci et al., 2008) How does docking of Cox17 onto Mia40 work?

To address this, we generated single Cys to Ser mutants for each Cys of the CX9C motifs of human COX17, the substrate studied before in the interaction with MIA40 (Banci et al., 2009). Wild-type COX17 was imported efficiently in isolated yeast mitochondria (Fig. 1 A, lanes 3–7), and the oxidized and reduced species were resolved, with the oxidized form increasing with a concomitant decrease of the reduced form. Additionally, a yMia40–COX17 mixed disulfide intermediate was observed, was coimmunoprecipitated with anti-Mia40 antibodies (Fig. 1 A, lanes 8–10), and was β-mercaptoethanol (β-Me) sensitive, as expected. This intermediate was resolved also under native conditions in blue native (BN)–PAGE (Fig. 1 B, 140-kD band; similar to small Tims; Milenkovic et al., 2007; Sideris and Tokatlidis, 2007). This was DTT sensitive and Mia40 specific, as clearing detergent-solubilized mitochondria with anti-Mia40 antiserum (but not preimmune serum) and protein A–Sepharose beads removed the 140-kD band specifically but not the unassembled Cox17 imported monomer (Fig. 1 B, lanes 4 and 5).

These assays were performed for each single Cys mutant of the CX9C motifs (Fig. 1 D). Only the mutant in the third Cys (C45S), which pairs with the second one (C36-C45; Fig. 1 C), was substantially affected (Fig. 1 D). Moreover, mutants of the Cys involved in copper(I) binding (C23 and C24l; Banci et al., 2008) were unaffected in forming the Mia40 intermediate (Fig. 1 D, first panel; also confirmed by BN-PAGE in Fig. S1). The severe defect of the C45S mutant was also clear in BN-PAGE (Fig. S1, lanes 9–11), whereas all other mutants were unaffected.

In multiple Cys mutants of COX17, the Mia40 intermediate was essentially abolished only when the third Cys was mutated (mutants C36/45S, C26/45/55S, and C36/45/55S; Fig. 1 E). Furthermore, when all other cysteines except C45 were mutated (C26/36/55S), covalent binding to Mia40 was unaffected, confirming the crucial and specific role of C45 in docking to Mia40 (Fig. 1 E).

Previously, Heaton et al. (2000) showed that for yeast Cox17, the fourth Cys of the twin CX9C motifs (i.e., C57, which is equivalent to C55 of hCOX17) was essential in vivo. Therefore, we addressed whether yCox17 differed from hCOX17 in the Cys docking to Mia40. The results (for single and multiple mutants of yCox17) are shown in Fig. S2. We find that interaction of yCox17 with Mia40, in fact, depends on the fourth Cys (C57), which is in agreement with its essential role in vivo (Heaton et al., 2000).

The data on human and yeast Cox17 show that Cox17 docks to Mia40 differently from the small Tims. This is a conundrum. How can different substrates be recognized by Mia40 in a strict site-specific manner yet involving different cysteines in each case?

Deletion analysis of Tim10 reveals an internal targeting signal for the Mia40 pathway

We thought that there must be a specific targeting signal in the substrate that guides its precise positioning to Mia40. In this way, a defined substrate Cys could be juxtaposed to the Mia40 active site Cys to make the crucial intermolecular disulfide. To identify such a putative targeting signal, we applied N- or C-terminal end deletion analysis on Tim10 (Fig. 2 A), ^{35}S labeled the Tim10 variants, and imported them into wild-type mitochondria (the lysate input controls are in Fig. S3). Mia40 interaction was monitored by the presence of a β-Me–sensitive intermediate (Fig. 2 B). Increasingly longer deletions of the N-terminal end showed a defect in making the Mia40 intermediate, which was completely abolished when residues 30–39 were deleted. In contrast, all C-terminal end deletions (lacking 21, 33, or 43 residues) were unaffected. Detecting the substrate released after interaction with Mia40, we saw that ΔN14 and ΔN30 were released in oxidized form. In contrast, ΔC33 and ΔC43 still bound to Mia40, but they were stalled in this interaction and could not be released. Presumably, this is because they lack the crucial third and fourth Cys (C61 and C65) that partner with C44 and C41 to make the folded oxidized species thus released from Mia40 (Sideris and Tokatlidis, 2007). This analysis suggested that (a) the N-terminal end segment 30–39 is crucial for targeting to Mia40 and (b) the region 14–30 facilitates targeting but is not crucial on its own. The loss of import capacity of the ΔN39 construct could be explained in two ways: (1) either it cannot cross the OM, or (2) it can cross the OM but can no longer bind to Mia40. To investigate the latter,

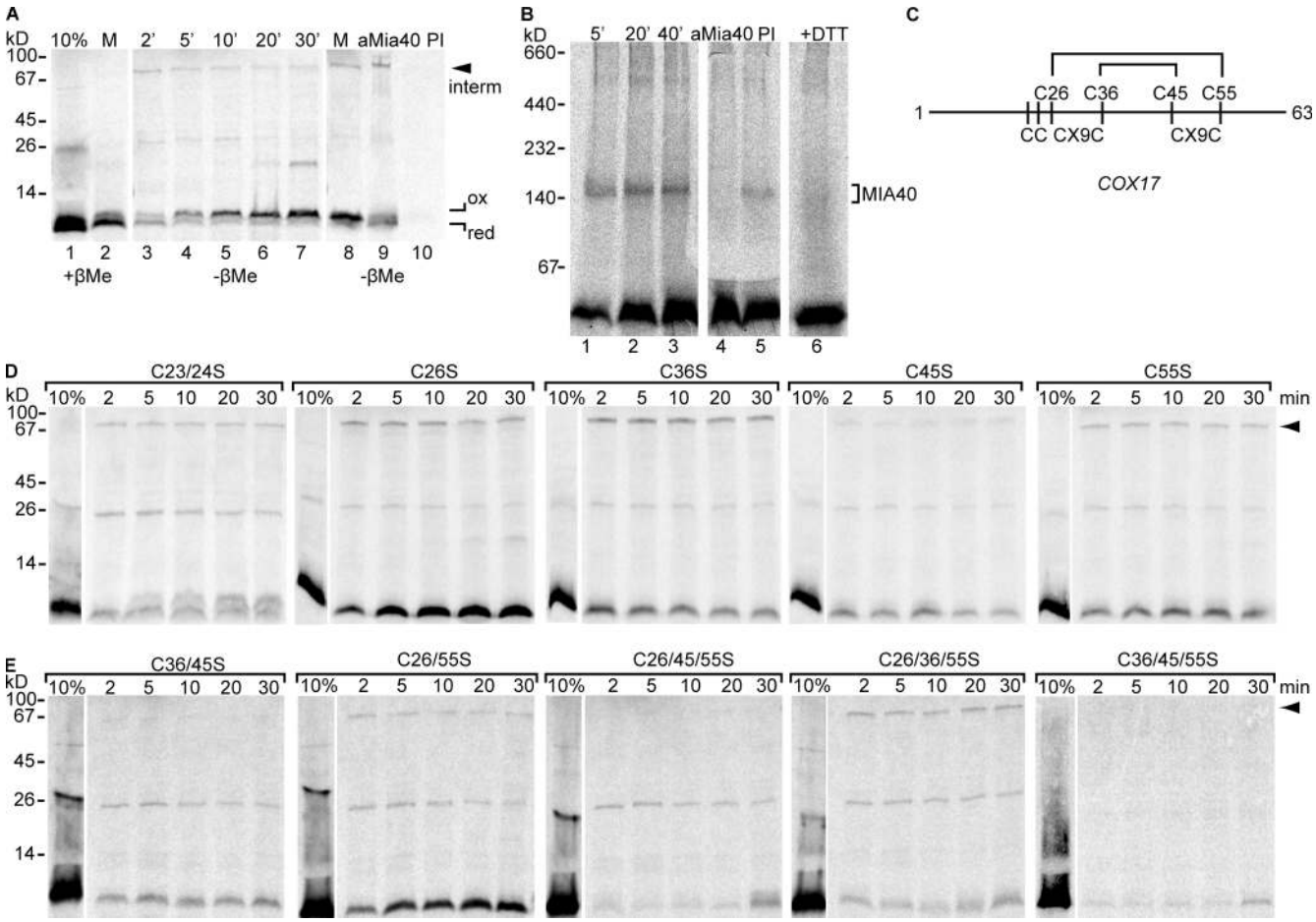

Figure 1. **Differential requirement of COX17 Cys residues for interaction with Mia40.** (A) ^{35}S-labeled COX17 import and immunoprecipitation as indicated, followed by SDS-PAGE. (B) As in A but using BN-PAGE. (C) Cys organization of COX17. (D) As in A for single Cys mutants. (E) As in D for multiply mutated Cys. (A, D, and E) Arrowheads indicate the Mia40 mixed intermediate (interm).

we tested in vitro binding of the Tim10 constructs (in radioactive form) to pure Mia40 (bead immobilized; Fig. 2 C). The results are identical to the import results showing decreased binding when the first 30 residues are missing (ΔN30) and complete loss of binding when a further nine residues are missing (ΔN39).

To verify that the observed defect for ΔN39 is relevant in vivo, we directed this construct to the IMS by fusion to the presequence of cytochrome b_2 (cyb2; residues 1–85), which targets precursors to the IMS independently of Mia40. In this way, any putative defects of ΔN39 in crossing the OM are bypassed, and this domain now targeted to the IMS can interact with Mia40 in its physiological environment. The fusion cyb2(1–85)ΔN39Tim10 could be efficiently imported into both wild-type– and Mia40-depleted mitochondria (Fig. 2 D) but did not give a Mia40 intermediate. This strongly argues that the ΔN39 deletion affects the interaction with Mia40 in organello, which is in agreement with the in vitro data.

Therefore, the segment 30–39 of Tim10 directly mediates binding to Mia40 and functions as a Mia40-specific ITS. By comparison, the MISS signal reported by Milenkovic et al. (2009) was defined by residues 35–43.

The MISS/ITS is conserved among the small Tims

To test whether the ITS is conserved in other small Tims, corresponding deletions in Tim9 and -12 were made. In Tim9, deleting 23 residues from the N terminus affected the interaction with Mia40 upon import to an extent, but deleting the putative MISS/ITS (ΔN34) completely abolished the interaction (Fig. 3, A and B). For Tim12, the deletion ΔN28 was reported previously to be import deficient (Fig. 3 C; Lionaki et al., 2008), which could be caused by a defective import through the OM or defective interaction with Mia40. As in this construct the putative Tim12 MISS/ITS is intact (residues 29–39; Fig. 3 A), we expected it to still bind to Mia40 if directed to the IMS as a cyb2 fusion. In fact, a time-dependent Mia40 intermediate was seen for such a construct (Fig. 3 D, arrowheads), which was abolished in Mia40-depleted mitochondria (prepared from a galactose (GAL)-Mia40 strain; Banci et al., 2009), confirming that the ΔN28 can indeed interact with Mia40. When the putative MISS/ITS segment between residues 29 and 39 was deleted in ΔN39Tim12 fused to the cyb2(1–85) presequence, the interaction with Mia40 was completely abolished (Fig. 3 E), proving that the MISS/ITS of Tim12 segment 29–39 is necessary for Mia40 binding. The two cyb2 fusion constructs

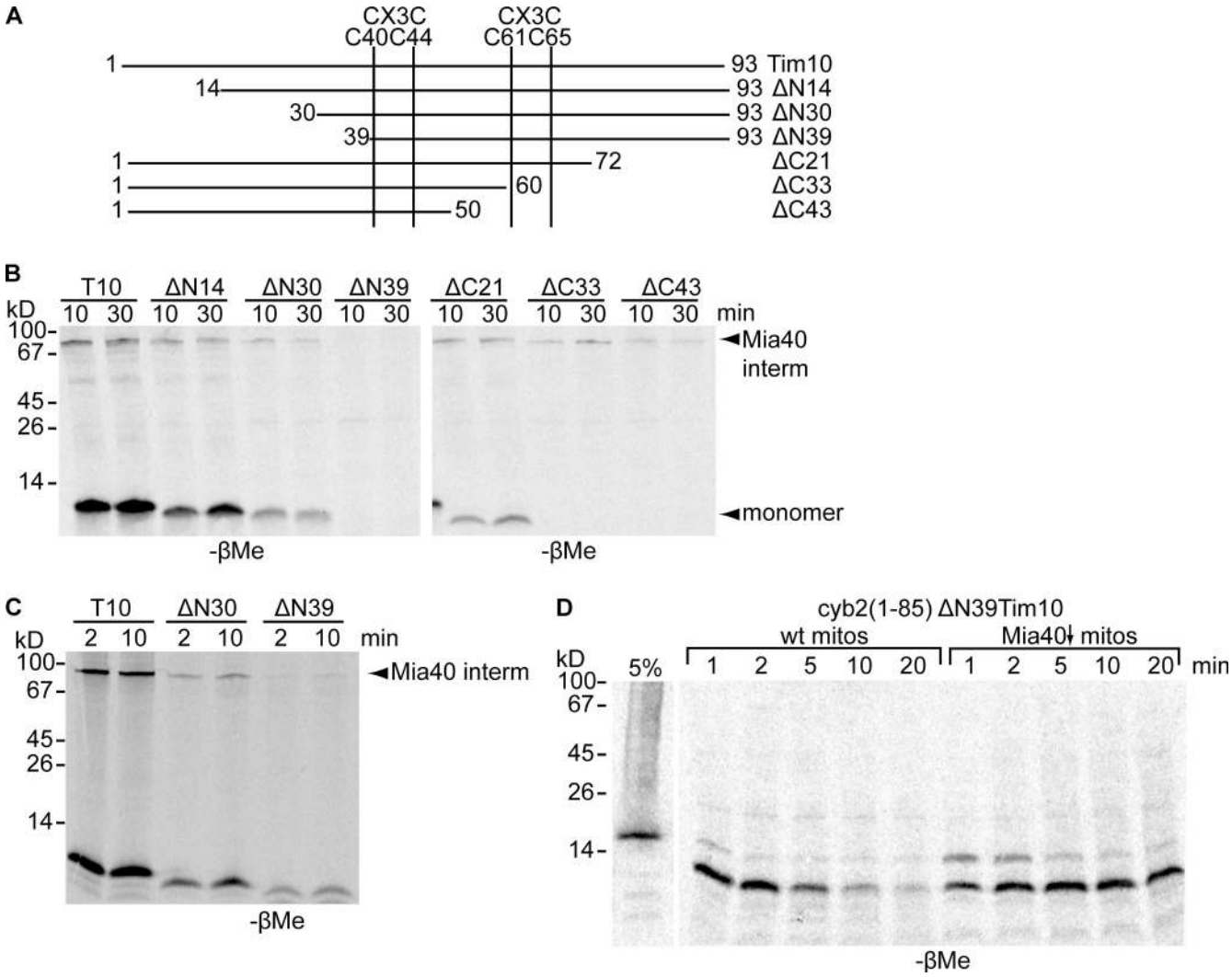

Figure 2. **Deletion analysis of Tim10 reveals an internal targeting signal for the Mia40 pathway.** (A) Tim10 truncations. (B) Import and analysis of Tim10 versions as in Fig. 1 A. (C) GST-Mia40 pull-downs of different Tim10 versions (as in Sideris and Tokatlidis, 2007). (D) Import of cyb2(1–85)ΔN39Tim10 in wild-type (wt) and Mia40-depleted (Mia40↓; Banci et al., 2009) mitochondria (mitos). interm, intermediate.

to ΔN28Tim12 and ΔN39Tim12 allowed us to uncouple the import to the IMS from the Mia40 interaction and to test whether this interaction is essential in vivo by complementation assays in yeast cells (Fig. 3 F). cyb2(1–85)ΔN28, which bears the MISS/ITS and interacts with Mia40, could restore viability substantially, arguing that the interaction with Mia40 is a functional one. In contrast, the cyb2(1–85)ΔN39 lacking the MISS/ITS and not interacting with Mia40 could not restore growth despite proper targeting to the IMS.

Collectively, these data suggest that the presence of MISS/ITS upstream of the N-terminal end Cys is conserved for Tim9 and -12. Furthermore, they show that the MISS/ITS-mediated interaction with Mia40 is essential in vivo.

Critical residues and consensus motif of the MISS/ITS

To identify the critical residues for the functionality of the MISS/ITS, Ala-scanning mutagenesis was performed (Fig. 4), in which residues of the MISS/ITS peptide 32–39 of Tim10 were exchanged to Ala (Fig. 4 A) and tested for Mia40 interaction (Fig. 4 B). Replacing M32 and N34 in the double Ala mutant (2Ala) only partially decreased the interaction with Mia40, which was completely abolished when four, six, or seven residues were exchanged for Ala. Because the 2 aa that were mutated in the 4Ala mutant additionally to the 2Ala mutant were F33 and K35, we tested these as single amino acid substitutions (Fig. 4, C and D). Exchanging F33 to Ala completely abolished the Mia40 intermediate, whereas K35A had only a minor effect. L36A was affected to a substantial degree compared with the wild-type but was clearly not as critical as F33. The complete loss of intermediate in the F33A/L36A double mutant can be attributed to the effect of F33A mutation alone. Identical results were obtained when the MISS/ITS mutants were used in Mia40-binding experiments in mitoplasts (bypassing translocation across the OM), which thus reflects a specific interaction with Mia40 (Fig. 4 E). Collectively, the Ala mutagenesis

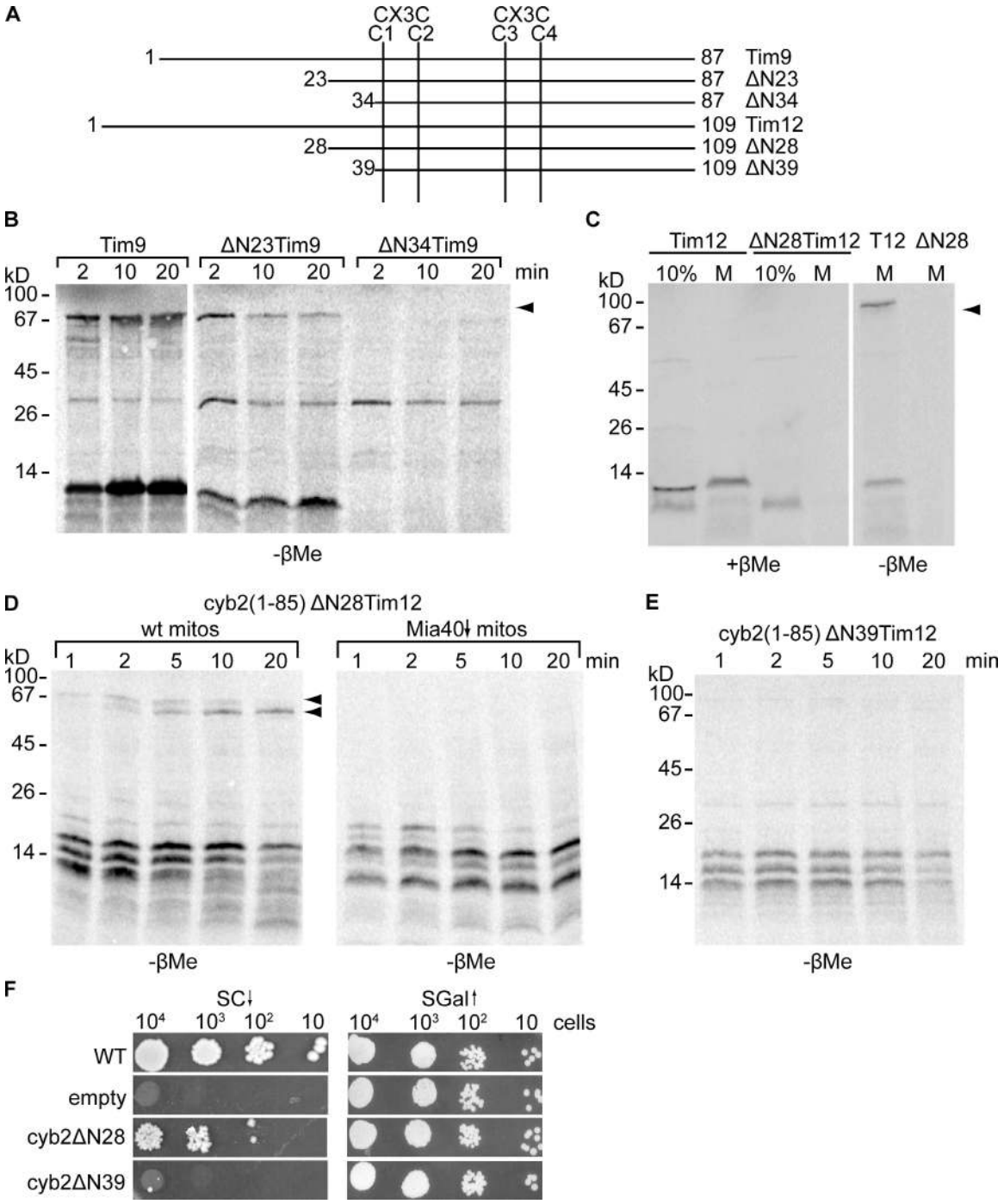

Figure 3. **The Tim10 ITS is conserved among small Tims.** (A) Tim9 and -12 truncations. (B) The intermediate with Mia40 is shown by an arrowhead. (C) As in B for Tim12 variants. 10% of in vitro translation mix was loaded as a standard. M, total mitochondria reisolated after import and protease treatment. (D) Import of cyb2(1–85)ΔN28 Tim12 fusion as in B. (C and D) Arrowheads indicate the Mia40 mixed intermediate. mitos, mitochondria; wt, wild type. (E) As in B but for the ΔN39Tim12 fragment. (F) In vivo complementation of *Tim12* fusion variants using a *GAL-Tim12* strain as described previously (Lionaki et al., 2008). SGal, GAL media; SC, glucose media; WT, wild type.

identified F33 (at position −7 relative to the docking Cys) and L36 (at position −4) as the two important residues in the MISS/ITS, with F33 being absolutely critical. Both of these residues are conserved (there are either identical or chemically similar residues in these positions) in the consensus MISS/ITS sequence X[Ar]XX[Hy][Hy]XXC described in this study (Fig. 4 F and Fig. S3).

Structural basis of the MISS/ITS interaction with Mia40

How is the targeting function of the MISS/ITS linked to the requirement for Cys-specific docking onto Mia40? Because Mia40 recognizes substrates in a Cys-dependent manner, precise positioning of the substrate Cys must be guided by a folded MISS/ITS in a conformation-dependent manner to control

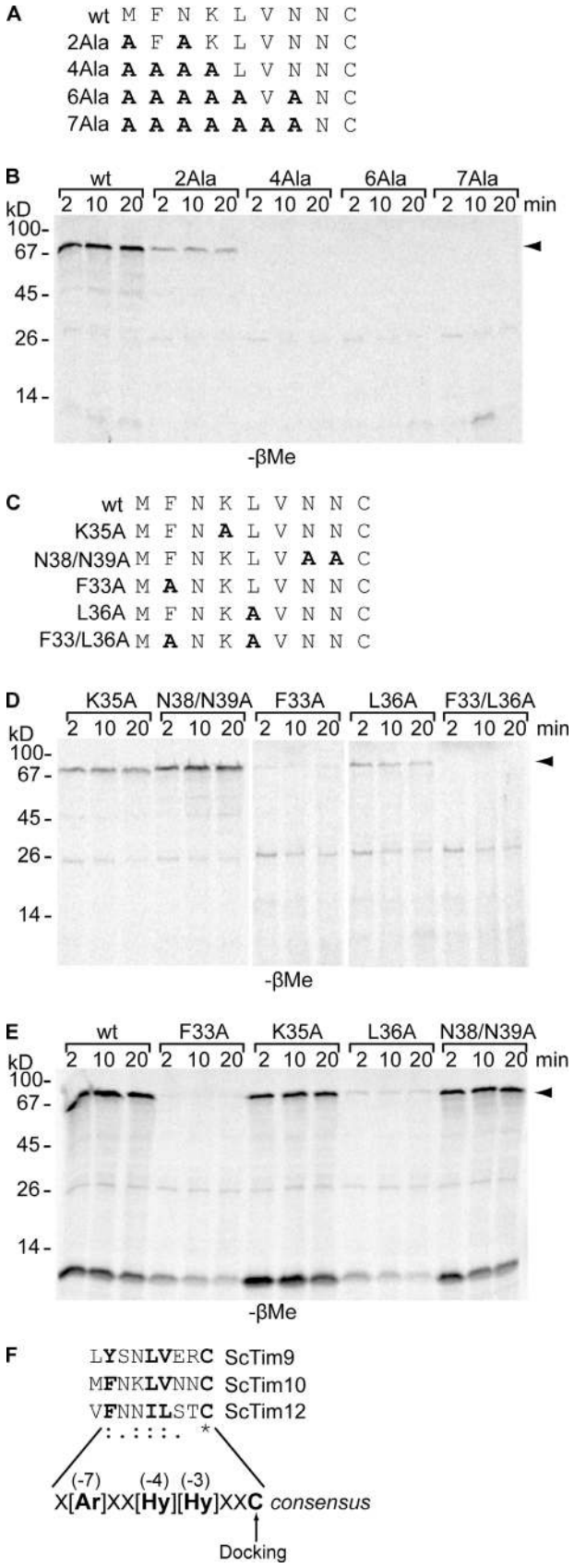

Figure 4. **Ala mutagenesis identifies critical residues of the ITS.** (A) The ITS of Tim10 with Ala substitutions (bold). (B) Imports of Tim10 Ala mutants performed as in Fig. 1. (C) Targeted Ala substitutions (bold) in the ITS of Tim10. (D) Import assays of the mutants of C. (E) As in D, but precursors were presented to mitoplasts. (B, D, and E) Arrowheads indicate the Mia40 mixed intermediate. (F) Alignment of the ITS sequence (residues 30–40 upstream of the N-terminal C40 in Tim10) in *S. cerevisiae* Tim9, -10, and -12. The consensus ITS sequence and the Cys docking to Mia40 are shown. The critical residues for the functionality of ITS are bolded, with their position relative to the docking Cys in parentheses. Colons indicate that conserved substitutions are observed, periods indicate that semiconserved substitutions are observed, and the asterisk indicates that the residues or nucleotides in the column are identical in all sequences in the alignment. wt, wild type.

optimal attachment to Mia40. When projected in a helical wheel (Fig. 5 A), the MISS/ITS forms an amphipathic α helix with the docking Cys sitting adjacent to the critical aromatic residue of position −7 on the same hydrophobic face that is made by the functionally important residues at positions −7, −4, and −3, whereas the hydrophilic side contains charged residues that are dispensable for function. The MISS/ITS is indeed helical in the crystal structure of the human and yeast Tim9–Tim10 complexes (Webb et al., 2006; Baker et al., 2009). Although the structure of Tim9 and -10 as they interact with Mia40 is unavailable, the helical conformation of MISS/ITS and the nature of its residues could explain in structural terms its specific interaction with the hydrophobic substrate-binding domain cleft of MIA40 (Banci et al., 2009). To test this concept, we produced a theoretical modeling of the Tim9 and -10 docking to the Mia40 cleft using the HADDOCK program (Dominguez et al., 2003). Only one cluster of structures was obtained for both TIM9–MIA40 and TIM10–MIA40 calculations containing 195 and 182 over 200 structures with a backbone root mean square difference to the mean structure for the structured region of the proteins of 1.5 Å and 1.3 Å, respectively. The buried surface area obtained is 2,090 ± 60 $Å^2$ for the TIM9–MIA40 complex and 1,471 ± 36 $Å^2$ for the TIM10–MIA40, which are indicative of a very good surface complementarity between the ITS and the binding cleft of Mia40 (Fig. 5 B, cloud of pink dots). The orientation of the hydrophobic face of the MISS/ITS amphipathic helix is underpinned by aromatic–aromatic and aliphatic–aliphatic interactions between the functionally important Tim residues (Fig. 5 B, gray) and hydrophobic residues of Mia40 (cyan). Additionally, the length of the substrate-binding cleft of Mia40 accommodates precisely the 9-aa long MISS/ITS helix, at the end of which the docking Cys of the substrate engages in the disulfide bond with the Mia40 Cys (Fig. 5 B, yellow spheres). The modeling presented in this study supports the recognition of the MISS/ITS as a folded helix by Mia40.

To scrutinize this concept experimentally, we used Cys-scanning mutagenesis of the docking Cys of Tim10 (C40). The underlying idea is that if the crucial docking Cys lies within an unfolded segment, moving it by up to four residues upstream or downstream would not substantially affect binding to Mia40. In contrast, if the docking works in the context of a folded MISS/ITS helix, moving the Cys away from the wild-type position would put it in a completely opposite side of the helix, strongly affecting its interaction with the facing Cys of Mia40. Thus, variants of Tim10 with a unique Cys in each of four positions upstream or downstream of the wild-type position 40 to span a full helix turn were produced, starting from a Tim10 in which

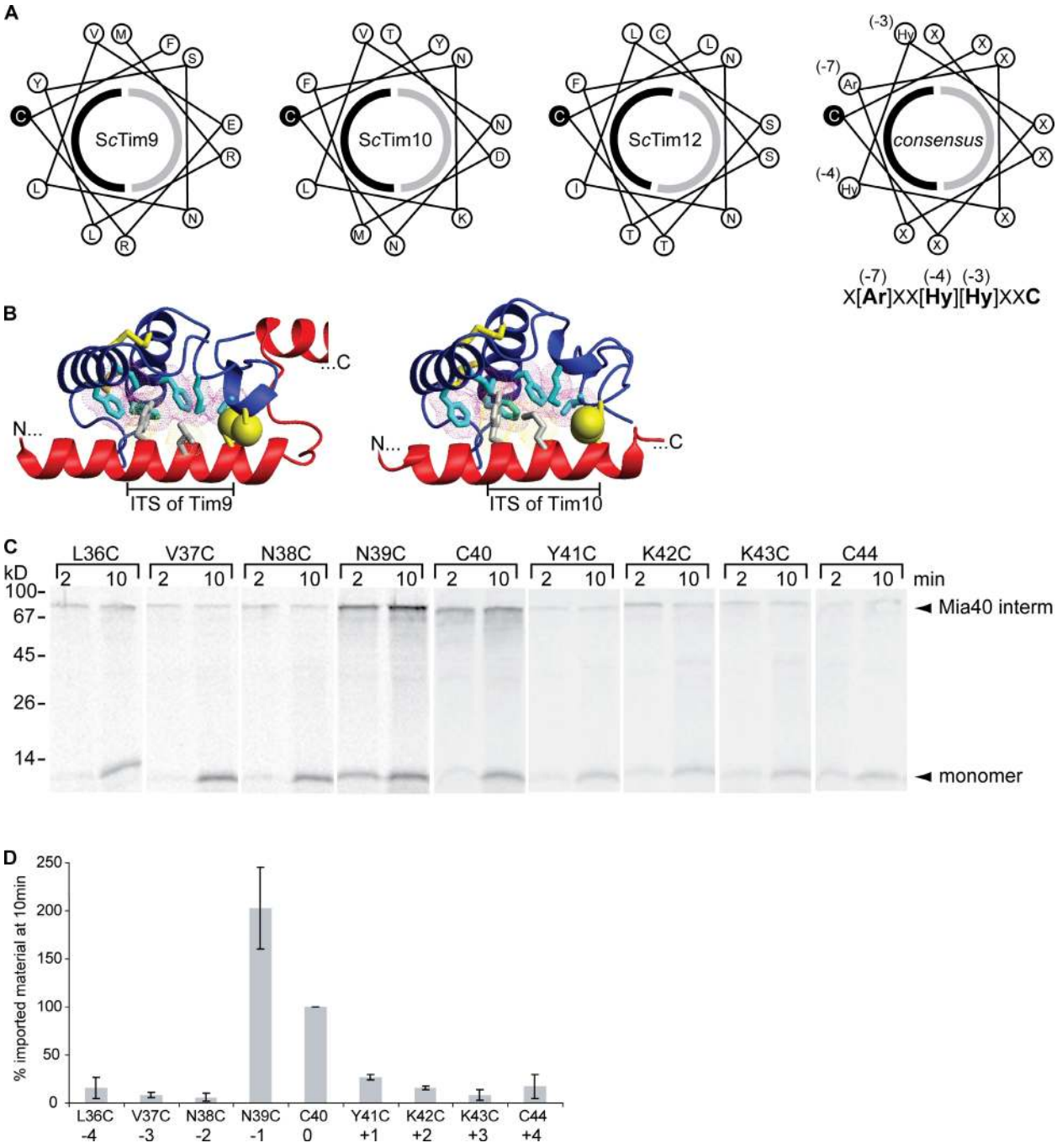

Figure 5. **Cys-scanning mutagenesis and conformational properties of the ITS.** (A) Helical wheel representation of ITS in *S. cerevisiae* Tim9, -10, and -12. The hydrophobic (black) and hydrophilic (gray) faces of the helix are indicated as half circles. (B) Theoretical modeling of hTIM9 and hTIM10 docking to the hMIA40 substrate–binding cleft using HADDOCK. TIMS and MIA40 are shown as red and blue ribbons, respectively. Hydrophobic residues of MIA40 interacting with TIMS are in cyan. Conserved aromatic and hydrophobic residues in the first helix of the TIMS interacting with the MIA40 hydrophobic cleft are in gray. Cysteines are in yellow, and the docking cysteines of the TIMS and MIA40 are shown as yellow spheres. (C) Cys substitutions in Tim10 and import and Mia40 intermediate (interm) analysis. (D) Quantification of the Mia40 intermediate after 10-min import (three independent experiments). Error bars represent standard error of the mean.

all cysteines were exchanged to Ser. Previously, a mutant carrying only the wild-type docking Cys (C40) was shown to maintain the interaction with Mia40, as C40 is necessary and sufficient (Milenkovic et al., 2007; Sideris and Tokatlidis, 2007). The mutants with the unique Cys in positions 36, 37, 38, and 39 or 41, 42, 43, and 44 were tested for the formation of the Mia40 intermediate after import (Fig. 5 C). All of the mutants completely lost the ability to form a disulphide intermediate with Mia40, with the exception of C39, which showed an increased amount of the intermediate. Therefore, changes in the positioning of the docking C40 are generally not tolerated for the interaction with Mia40. Overall, the Cys-scanning mutagenesis suggests that Cys docking depends on the folding of MISS/ITS into a helix that appropriately positions it opposite the partner Cys of Mia40.

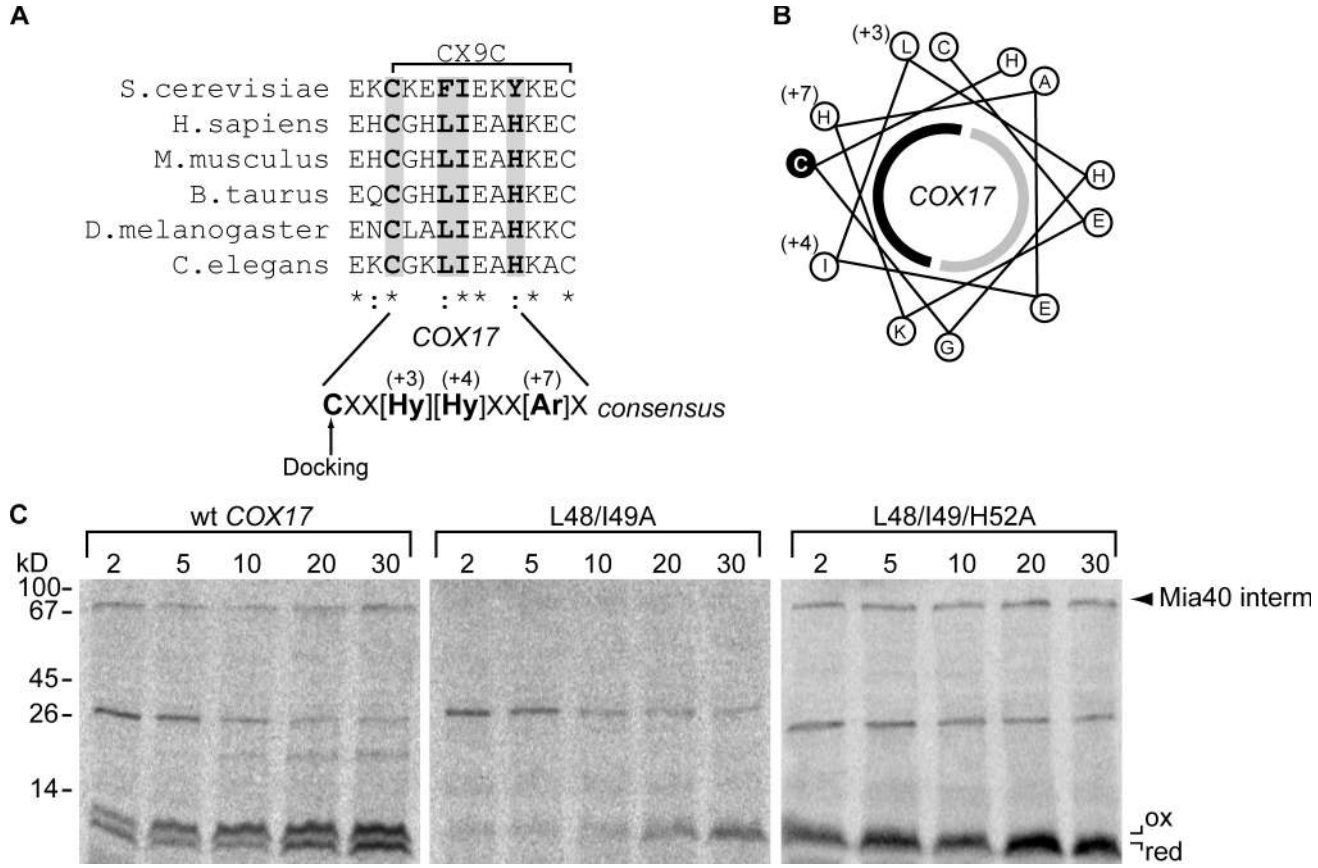

Figure 6. **An ITS is present in the C-terminal end of Cox17.** (A) Alignment of Cox17 ITS sequences from different eukaryotes. Strictly conserved residues in the ITS consensus are shaded gray and bolded. Colons indicate that conserved substitutions are observed, and asterisks indicate that the residues or nucleotides in the column are identical in all sequences in the alignment. (B) Helical wheel projection for the ITS of COX17 as in Fig. 5 A. (C) COX17 mutants were imported and analyzed for mixed disulfide intermediate (interm) with Mia40 (arrowhead). wt, wild type.

A MISS/ITS is present at the C-terminal end of Cox17

Is there a MISS/ITS present in Cox17 as well? Sequence alignment of Cox17 and small Tims does not reveal a MISS/ITS upstream of the COX17 docking C45, as would be expected by analogy to the Tims. However, such a motif became apparent downstream of the COX17 docking C45 (Fig. 6 A). Strictly conserved residues in this segment were at equal distances from the docking C45 as in the MISS/ITS of small Tims but downstream (positions 3, 4, and 7) and were thus aligned in the same face of the helical wheel projection with the docking Cys (Fig. 6 B). Therefore, this important structural feature of the MISS/ITS is maintained. To test whether the COX17 MISS/ITS is indeed functional, the Leu and Ile at positions 3 and 4 in COX17 (and conserved among Cox17 sequences) were mutagenized. This double mutant could not form a Mia40 intermediate (Fig. 6 C). At position 7, there is a Tyr in *Saccharomyces cerevisiae* Cox17 (also maintained as a Phe/Tyr in the small Tims at position −7), but this is a His in all higher eukaryotic Cox17 sequences. Mutating this His to Ala in COX17 in a triple L48/I49/H52A mutant showed a striking gain of function effect producing more intermediate with Mia40, arguing for the importance of a hydrophobic/aromatic residue in position 7. We should note two things concerning COX17: (1) the reduced COX17 shown to interact with MIA40 by nuclear magnetic resonance (Banci et al., 2009) maintains a secondary structure content similar to the folded COX17 as measured by circular dichroism (Banci et al., 2008), and (2) a theoretical docking between COX17 and MIA40 similar to that performed in this study for the small Tims and Mia40 supports a good surface complementarity between the MISS/ITS segment of COX17 and MIA40 (Banci et al., 2009).

How can the MISS/ITS work in the case of yeast Cox17 in which the docking Cys is the fourth one? In the MISS/ITS sequence between Cys3 and -4 for the yeast protein (Fig. 6 A, first line), there is a Phe, Ile, and Tyr at positions 3, 4, and 7 after the third Cys, rendering this region similar to the consensus MISS/ITS of the small Tims (that has no His in position 7). Intriguingly, the other residues in this region of the yeast Cox17 all form pairs of opposite charges (four pairs of Lys and Glu), which could interact through salt bridges and allow the Phe, Ile, and Tyr to properly position the MISS/ITS in the cleft of Mia40. In this case, the yCox17 MISS/ITS functions upstream of the docking C57. Therefore, it appears that although there is a MISS/ITS in Cox17 that maintains the general structural features of the MISS/ITS, it functions downstream of the docking Cys for hCOX17 or upstream of the docking Cys for yCox17.

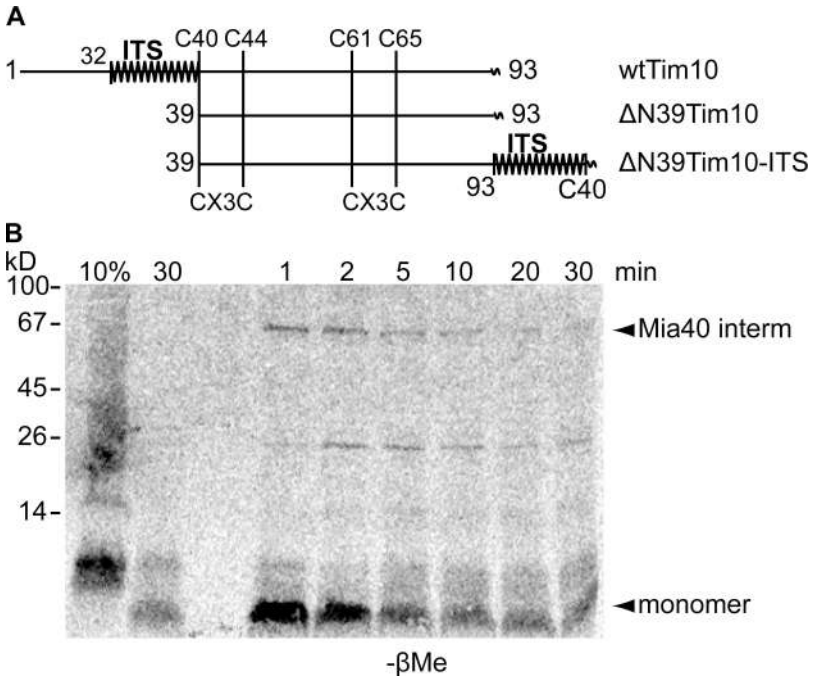

Figure 7. **Swapping the ITS from the N- to the C-terminal end of Tim10 does not affect targeting.** (A) Schematic representation of the Tim10 ITS (zigzag line) and C-terminal end fusion to ΔN39Tim10. wt, wild type. (B) ΔN39Tim10-ITS was imported and analyzed for mixed disulfide intermediate (interm) formation with Mia40.

Docking calculations using the data-driven docking program HADDOCK were performed to investigate the basis for selecting a different Cys in the Cox17–Mia40 complex formation in yeast with respect to human. Calculations were performed on both the yeast and human Mia40–Cox17 complexes in which the second Cys of the CPC motif of Mia40 was bound through a disulphide to either the C3 (Cys47 in COX17 or Cys45 in yCox17) or C4 (Cys57 in COX17 or Cys55 in yCox17) of Cox17, thus resulting in two types of complexes for each organism. From the analysis of the data (Table S1), it emerges that the yMia40–yCox17 complex involving C4 of yCox17 (HADDOCK score −152.7) has, by far, a much better score than that involving C3 (cluster 1, HADDOCK score −127.4; cluster 2, HADDOCK score −121.3). On the contrary, the hMia40–hCox17 complex involving C3 of hCox17 (HADDOCK score −88.7) has a better score than that involving C4 (cluster 1, HADDOCK score −66.6; cluster 2, HADDOCK score −56.0). Therefore, the docking data completely match the experimental results. From the comparison of the structural models of the best complexes for the two systems (i.e., yMia40−yCox17 complex involving C4 of yCox17 vs. hMia40−hCox17 complex involving C3 of hCOX17), it appears that their different interaction mode is dictated by the nature and steric hindrance of the residues of the MISS/ITS stretch involved in the interaction with the hydrophobic cleft of Mia40. Indeed, a Phe in yCox17 is changed to a Leu in hCOX17, and a Tyr in yCox17 is changed to a His in hCOX17. In particular, the Tyr in yCox17 is positioned close to two Phe residues of the Mia40 cleft, possibly engaging in strong stacking interaction, thus favoring the C4 interaction mode in yeast (Fig. S4). These results support the generality of the function of a MISS/ITS-dependent targeting mechanism for other substrates of the Mia40 pathway unrelated to the small Tims.

Swapping the MISS/ITS from the N- to the C-terminal end of Tim10 does not affect targeting

The presence of the MISS/ITS at the C-terminal end of Cox17 rather than at the N-terminal end, as for the small Tims, suggested that its targeting function is independent of localization within the protein. Indeed, fusion of the ITS to the C terminus of the import-incompetent ΔN39Tim10 (Fig. 7 A) restored import as well as its capacity to make a Mia40 intermediate (Fig. 7 B). Thus, the MISS/ITS can exert its targeting function independently of its localization within the targeted polypeptide. However, despite efficient import and interaction with Mia40, the ΔN39Tim10-ITS fusion was rapidly degraded after import (in contrast to wild-type Tim10), presumably because of incomplete or improper folding. This behavior is reminiscent of the cyb2(1–85)ΔN39Tim10 (Fig. 2 D). Therefore, the MISS/ITS in ΔN39Tim10-ITS is sufficient for translocation across the OM and for docking to Mia40, but it cannot lead to productive folding. The latter can apparently only occur when the MISS/ITS is properly positioned N-terminally to the CX3C motifs.

The MISS/ITS can target Mia40-independent and nonmitochondrial proteins to the organelle

We wanted to know whether the MISS/ITS can target efficiently (a) mitochondrial proteins that are not substrates for Mia40 and (b) nonmitochondrial proteins. We first used Sue of ATPase (subunit e of yeast mitochondrial F1FoATPase), which is targeted to the inner membrane independently of Mia40 (Fig. 8 A; Tokatlidis et al., 1996; Everard-Gigot et al., 2005). Deletion of the N-terminal end transmembrane anchor (ΔN23Sue) abolished import of Sue. Fusion of the MISS/ITS of Tim10 to the N-terminal end of ΔN23Sue (with Sue lacking its unique endogenous C28 to avoid aberrant disulfides)

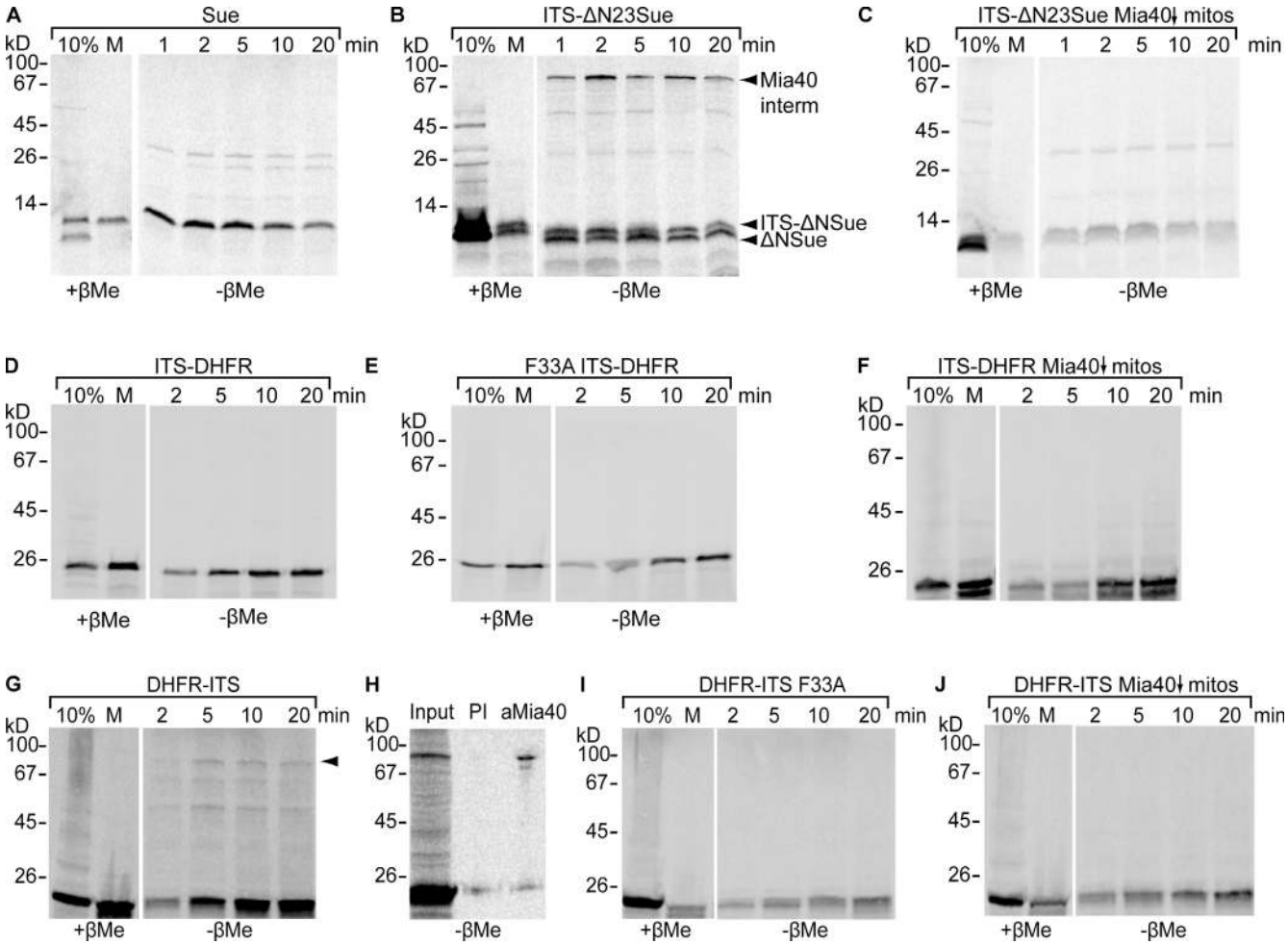

Figure 8. **Fusion of the ITS can target to mitochondrial Mia40-independent substrates and nonmitochondrial proteins.** (A) Import of Sue in wild-type mitochondria. (B) As in A for ITS-DHFR. interm, intermediate. (C) As in B but in Mia40-depleted mitochondria. (D) ITS-DHFR import as in A. (E) As in D but with the F33A Tim10 ITS mutant. (F) As in D but in Mia40-depleted mitochondria. (G) DHFR-ITS fusion and import as in D. The arrowhead indicates the Mia40 mixed intermediate. (H) Immunoprecipitation after the import of DHFR-ITS with anti-Mia40 or preimmune serum (PI). (I) As in G but with the F33A Tim10 ITS mutant. (J) As in G but in Mia40-depleted mitochondria.

restored import substantially (Fig. 8, A and B) and formed a β-Me–sensitive Mia40 intermediate (Fig. 8 B) not observed for wild-type Sue (Fig. 8 A). Consistently, the ITS-ΔN23Sue import decreased substantially, and no intermediate was formed in Mia40-depleted mitochondria (Fig. 8 C). The low but measurable amount of ITS-ΔN23Sue still imported in this case (and is thus Mia40 independent) is attributable to the ability of the MISS/ITS to direct import across the OM (see next two paragraphs). As interaction with Mia40 suggested localization in the IMS, we tested this directly (Fig. S5 A). The Mia40 intermediate and the monomeric ITS-ΔN23Sue were largely degraded in mitoplasts treated with protease, indicating that they are accessible in the IMS.

To address the capacity of MISS/ITS to target nonmitochondrial proteins to the organelle, we used mouse dihydrofolate reductase (DHFR), a small, well-folded protein used traditionally as a model in such experiments. As a control, fusion of the nontargeting 30 first residues of yeast ADP/ATP carrier N-terminally to DHFR did not allow significant import (Fig. S5 B). In contrast, a substantial amount of DHFR (around 10%; Fig. 8 D) was imported into mitochondria when fused with ITS at its N-terminal end, supporting the ability of MISS/ITS to target DHFR across the OM. However, no intermediate with Mia40 could be observed (Fig. 8 D), import was not affected when the mutant F33A ITS, which abolishes the interaction with Mia40 (Fig. 4 D), was used (Fig. 8 E), and finally, import into Mia40-depleted mitochondria was unaffected (Fig. 8 F). This suggested that although MISS/ITS ensured translocation across the OM, interaction with Mia40 did not occur or was not stable enough, which might lead to import into the matrix. Indeed, this was the case, as intramitochondrial localization of ITS-DHFR (Fig. S5 C) showed it remained intact in protease-treated mitoplasts (similar to the endogenous matrix protein cpn10).

Thus, appending the ITS to the N-terminal end of a nonphysiological substrate for Mia40 is sufficient for translocation across the OM, which illustrates an important new function for the MISS/ITS signal, which is apparently Mia40 independent. In authentic Mia40 substrates, the OM translocation function is coupled to the Mia40-dependent oxidative folding of the substrate. However, for nonmitochondrial proteins, although the

ITS is sufficient for OM translocation, subsequent interaction with Mia40 is not always guaranteed. Conceivably, the ITS may not be accessible enough in well-folded protein domains like DHFR to bind to Mia40. This can be rationalized on the basis that MISS/ITS is not present at the very N-terminal end of physiological Mia40 substrates and that sequences upstream of ITS could enhance the interaction with Mia40. We alternatively appended the ITS C-terminally to DHFR, as this could allow better accessibility of the ITS, which is in line with the result of ΔN39Tim10-ITS (Fig. 7). Indeed, the DHFR-ITS fusion protein interacted efficiently with Mia40 (Fig. 8, G–J). It formed a β-Me–sensitive intermediate upon import (Fig. 8 G) that was Mia40 specific (Fig. 8 H), abolished when the F33A mutant of ITS was used (Fig. 8 I), and absent from Mia40-depleted mitochondria (Fig. 8 J). Intramitochondrial localization experiments confirmed that DHFR-ITS is in fact localized in the IMS (Fig. S5 D).

MISS/ITS-dependent binding to Mia40 is mediated by hydrophobic interactions of micromolar affinity

The discovery of the ITS targeting to Mia40, the crucial role of the hydrophobic residues as shown by mutagenesis, and the structural requirement for these to be on the same side of the MISS/ITS helix (supported by the theoretical modeling and the Cys mutagenesis experiments) all point to a key role of hydrophobic interactions in this targeting process. These noncovalent hydrophobic interactions must be strong enough to properly orient the substrate so that disulfide bonding can then occur in a second step locking the interaction with Mia40. To directly test the importance of these noncovalent hydrophobic interactions, we (a) evaluated in binding experiments in vitro the effect of salt and detergent and (b) measured the thermodynamics of the ITS-mediated interaction of the substrate with Mia40 by isothermal titration calorimetry (ITC). For these experiments, we used ΔN290Mia40SPS, which (a) lacks the first 290 residues that are not important for interaction and dispensable in vivo (unpublished data) and (b) has both cysteines of the active site CPC exchanged to Ser so that it maintains its capacity for noncovalent interaction with the substrate without making the subsequent covalent disulfide bonding with the substrate.

Binding in vitro was tested in pull-downs of different radioactively labeled precursors onto pure, His-tagged ΔN290Mia40SPS immobilized on Ni beads. The results (Fig. 9 A) are in agreement with those from import assays. Wild-type Tim10 binds substantially as expected; deletion of the first 30 residues weakens binding to some extent, but entirely eliminating MISS/ITS (ΔN39) completely abolishes binding. Similar results were obtained with the ΔN23Sue precursor, for which substantial binding was detected only when the MISS/ITS was N-terminally fused to ΔN23Sue. Because this in vitro assay for noncovalent binding of precursors to Mia40 faithfully reflects binding in organello (Figs. 2 and 8), we tested the effect of salt and detergent in this assay. Salt did not seem to influence the interaction up to 500 mM NaCl (Fig. 9 B), confirming that ionic interactions are not crucial. In contrast, increasing detergent concentration weakened the interaction substantially (Fig. 9 C), arguing for a major role of hydrophobic interactions in the binding process. These data provide the first experimental support to the concept that the ITS–Mia40 interaction occurs primarily through hydrophobic interactions, underpinning the packing of the corresponding aromatic and aliphatic residues suggested by the theoretical docking in Fig. 5 B. They are also in full agreement with previous mutagenesis of the Mia40 substrate–binding cleft (Banci et al., 2009) and the mutagenesis of the substrate ITS presented in this study.

The thermodynamic noncovalent interactions between Tim10 and Mia40 were analyzed by ITC. As ITC data can be dominated by the strong energetic contribution of covalent bond formation, thus masking the lower contribution of noncovalent interactions, ΔN290Mia40SPS was used as explained in the previous paragraph. Tim10 was reduced as shown by AMS thiol-trapping experiments (Fig. S5 E). A clear interaction between ΔN290Mia40SPS (injected) and wild-type Tim10 (in the cuvette) was detected with a measured K_d of 3.3 μM ($3.3 \times 10^{-6} \pm 0.7 \times 10^{-6}$ M; ΔG −7.42 kcal/mol; Fig. 9 D, top left), which is consistent with a specific interaction in vivo. Deletion of the first 30 residues of Tim10 (ΔN30Tim10) lowered the affinity 19-fold (K_d ∼63 μM; $6.29 \times 10^{-5} \pm 0.14 \times 10^{-5}$ M; ΔG −5.68 kcal/mol; Fig. 9 D, top right), a value still consistent with a physiologically relevant interaction. However, deletion of a further nine residues, thus entirely cleaving the ITS, completely abolished the interaction (Fig. 9 D, bottom left; background binding with Mia40 injected alone to the buffer solution without any substrate in Fig. 9 D, bottom right). These results provide the first direct measurement of the affinity of the noncovalent interaction between Mia40 and one of its substrates, are in agreement with the binding data (Fig. 9 A), and correlate well with the import and interaction of the relevant versions of Tim10 with Mia40 in organello (Fig. 2 B).

Discussion

Previous analyses of the Mia40-dependent oxidative folding showed that Mia40 recognizes specific cysteines in this process based on studies with the small Tims showing that the first Cys of the CX3C motifs is crucial for docking (Milenkovic et al., 2007; Sideris and Tokatlidis, 2007). Binding of other substrates remained a conundrum. We report the surprising finding that Cox17, a CX9C substrate, docks to Mia40 via its third or fourth Cys of the twin CX9C motifs, which is in sharp contrast to the small Tims. This clear difference can now be rationalized in the light of our identification of a novel targeting signal (the ITS) that is conserved among small Tims and Cox17 and allows a particular Cys, different in each substrate, to dock to Mia40. The ITS has several defined features. It is a 9-aa peptide that is conserved among small Tims immediately upstream of their N-terminal end first Cys. The consensus sequence is X[Ar]XX[Hy][Hy]XXC. The Ar residue at position −7 relative to the first Cys is crucial as single mutagenesis of this residue abolishes targeting. The Hy at position −4 is also important but not crucial. The ITS tends to form a helix that aligns uncharged/hydrophobic residues (in particular Ar and Hy at −7 and −4 and −3) to the same side of the crucial docking Cys.

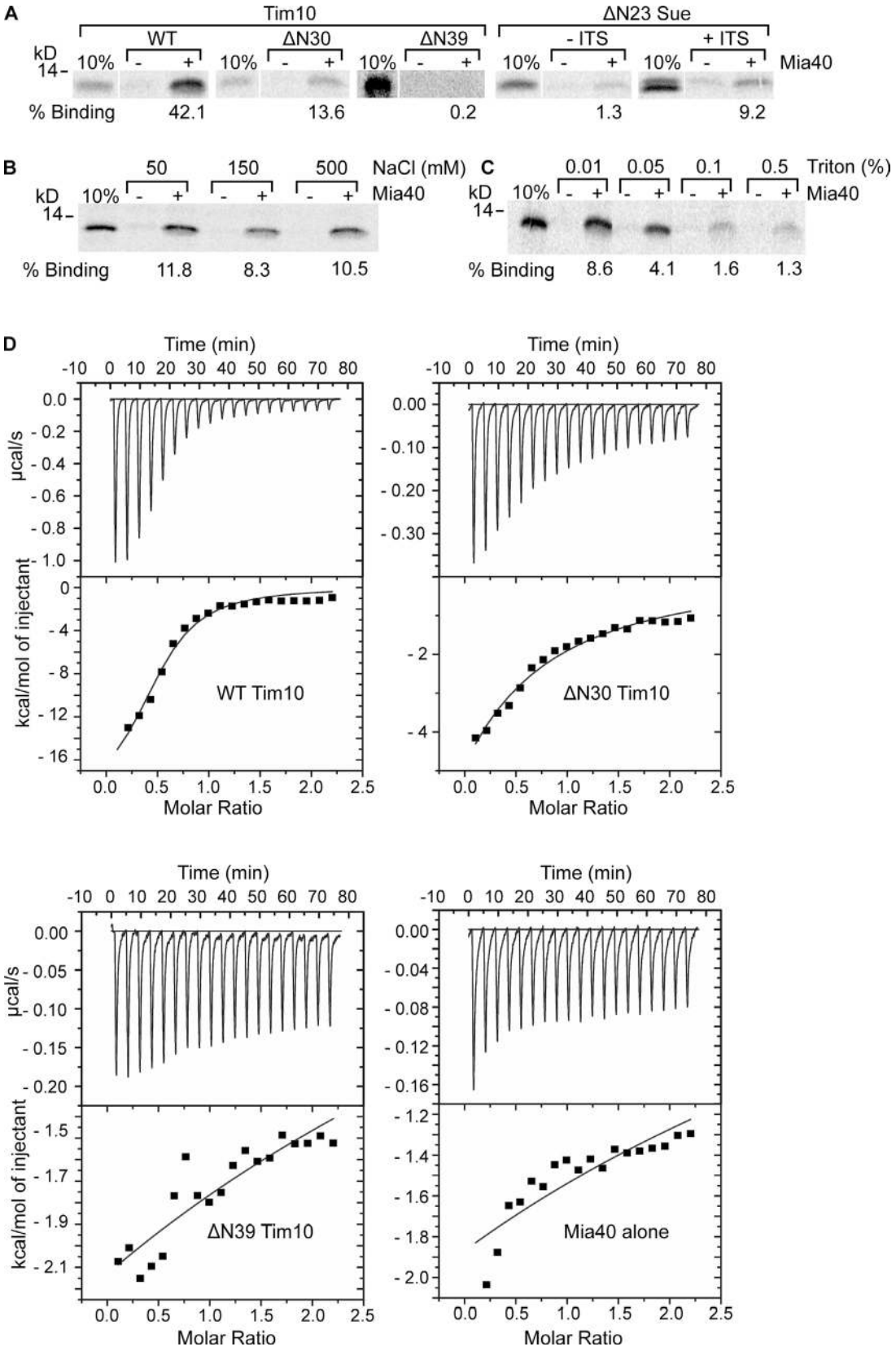

Figure 9. **The noncovalent ITS-dependent binding of substrates to Mia40 is mediated by hydrophobic interactions.** (A) Purified His-tagged ΔN290Mia40SPS was bound to Ni^{2+}-NTA beads. ^{35}S-labeled proteins were incubated with Ni-NTA beads with or without ΔN290Mia40SPS at 15°C for 2 h. (B) ^{35}S-labeled Tim10 was incubated with Ni-NTA bead–immobilized ΔN290Mia40SPS for 2 h at 30°C in the presence of 50, 150, or 500 mM NaCl. (C) As in B, but binding was performed in the presence of 0.01, 0.05, 0.1, or 0.5% Triton X-100. (D) ITC of 0.25 mM ΔN290Mia40SPS alone (bottom right) or with 0.025 mM of wild-type (WT) Tim10 (top left), Tim10 ΔN30 (top right), or Tim10 ΔN39 (bottom left).

A theoretical docking of the ITS onto the substrate-binding cleft of Mia40 shows (a) very good surface complementarity (buried surface area of 1,471 Å^2 or 2,090 Å^2 for TIM9–Mia40 and TIM10–Mia40 complexes, respectively) and (b) stabilizing hydrophobic interactions between the crucial elements of ITS and aliphatic side chains in the substrate cleft of Mia40. Cys-scanning experiments provided independent support to the concept that the ITS must fold in its interaction with Mia40. This structural, rather than simply sequential, feature of the ITS led us to look for such a signal in the vicinity of the docking Cys C45 of COX17, identifying it just downstream of C45, which is a striking result. Underscoring the importance of the precise nature of the residues in the ITS stretch, we found that in yCox17, this signal is oriented in such a way in the cleft of Mia40 that the last Cys of the twin CX9C motif is primed for docking to Mia40. The identification of the ITS for Cox17 agrees with the theoretical docking for a putative complex between COX17 and MIA40 (Banci et al., 2009). Interestingly, both Tims and Cox17 are oriented in the Mia40 substrate cleft similarly and perpendicularly to the two helices α2 and α3 of the Mia40 core. Also, the length of the ITS (9 aa) fits exactly to the substrate-binding cleft, ending up in the crucial Cys pair between the substrate and Mia40.

The variable positioning of the ITS in different Mia40 substrates suggested that it functions independently. Swapping the ITS to the C-terminal end of Tim10 without affecting targeting indeed proved this point. Further, fusing the ITS to either a mitochondrial protein that is not a substrate for Mia40 (Sue of ATPase) or a nonmitochondrial protein (DHFR) was sufficient for targeting. The results were more compelling in the case of a C-terminal fusion of the ITS to DHFR, presumably because in this case (as in the ΔN23TIM10-ITS), the ITS sequence is more accessible for binding to Mia40. The N-terminal end fusion ITS-DHFR retained the ability for complete translocation across the OM, illustrating this new role for the ITS, which is Mia40 independent. This analysis allowed us to uncouple the two events of translocation across the OM and Mia40-dependent folding, which are tightly coupled for authentic Mia40 substrates.

Having identified the ITS as the crucial targeting element in the Mia40 pathway, we checked for ITS-like signals in the known and predicted substrates of Mia40 (Table S2). The criteria for defining a sequence as a putative ITS were (a) a length of 9 aa upstream or downstream of the Cys and (b) the presence of one aromatic and one hydrophobic residue at positions 4 and 7. For the 15 known/predicted Mia40 substrates (Gabriel et al., 2007), we discovered at least one ITS identified (Table S2), with the exception of only yTim13. In light of the results for yeast and human Cox17, the putative ITS identified in Table S2 may be oriented in different ways in the cleft of Mia40. In any case, though, this signal primes a unique Cys for interaction with Mia40. Therefore, it appears that the presence of ITS is quite general. Furthermore, it appears that in CX3C substrates, ITS signals prime preferentially the first Cys for docking, whereas in CX9C substrates, this is less strict but with a preference for priming one of the C-terminal end cysteines.

The ITS expands the repertoire of mitochondrial-targeting signals. Its propensity to form an amphipathic helix is a common feature with the typical matrix-targeting signal, which may account for the capacity of ITS to cross the OM. In contrast, the ITS is much shorter, and its functionality relies mainly on the hydrophobic residues and the crucial Cys in contrast to the matrix-targeting signal, where both hydrophobicity and charge are important (Abe et al., 2000). One other ITS was reported for the cytochrome *c* heme lyase but is not present in other proteins and has very different properties from the ITS (∼60 residues long and strongly hydrophilic; Diekert et al., 1999). During preparation of our manuscript, Milenkovic et al. (2009) reported the identification of the MISS targeting signal in Tim9 and -10. This partially overlaps with the ITS signal sequence reported in this study, with good agreement between the data. In our study, identification of ITS in the small Tims provided the starting point to additionally (a) identify such a signal in different substrates, (b) solve the conundrum of how different substrates are recognized equally well by Mia40, and (c) dissect the structural and biophysical basis of this recognition process.

The noncovalent protein–protein interactions that are crucial for Mia40 binding and precede the covalent Cys docking were found to be primarily hydrophobic, as they were not affected by salt but were substantially competed by detergent in vitro. These results are in line with the theoretical docking experiments for a putative complex of different types of substrates (Tims or Cox17) with Mia40, in which hydrophobic packing of interacting residues seems to play a major role.

We measured for the first time the affinity of the noncovalent binding of the substrate to Mia40 by ITC. It was found that Tim10 had a strong noncovalent thermodynamic affinity to Mia40, indicating a specific recognition of Tim10 by Mia40 before the redox chemistry can take place. This also makes sense thermodynamically, as the subsequent interaction of a folded (oxidized) Tim10 with its partner Tim9 is two orders of magnitude stronger with a K_d of 30 nM (Lu et al., 2004), and thus, the entire process can be thermodynamically driven by a cascade of increasing affinities. The initial interaction that guides the substrate to Mia40 is mainly caused by the MISS/ITS, as cleavage of this segment (ΔN39Tim10) completely abolishes binding. The fact that binding is decreased but still measurable for ΔN30 suggests that the upstream 30 residues potentially stabilize the MISS/ITS structure for optimal interaction within the Mia40 cleft.

We propose a working model (Fig. 10) whereby the MISS/ITS has a dual function: first it guides the precursors through the OM, and then it orients them via hydrophobic interactions to the cleft of Mia40. The latter reflects the recognition by Mia40 (step 1: sliding step, ITS guided and noncovalent) and provides the basis for the receptor function of Mia40 in the IMS. Juxtaposition of the correct substrate-docking Cys to the active site Cys of Mia40 is a consequence of this initial recognition process, which thereby allows the correct disulfide to be formed (step 2: docking step, Cys dependent and covalently bound). Correct Cys priming in each substrate as determined by the ITS provides a mechanistic framework for the key role of Mia40 in the mitochondrial oxidative folding pathway.

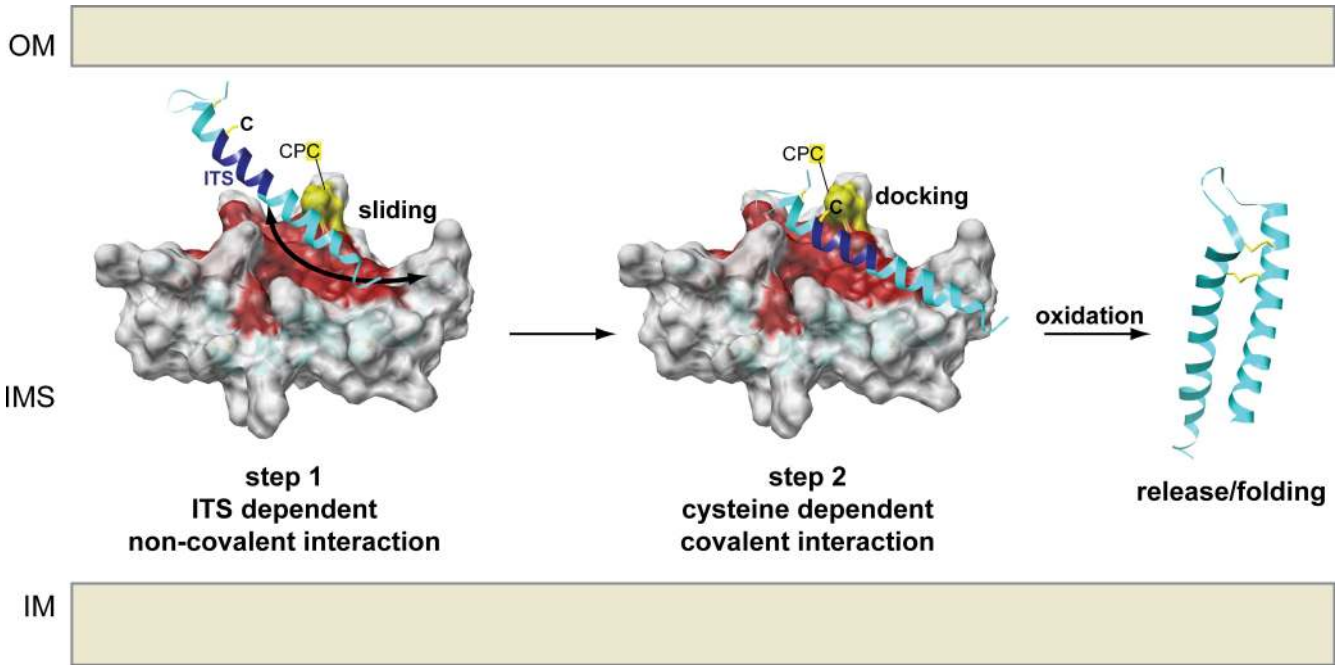

Figure 10. **Sliding–docking model for the interaction of substrates with Mia40.** (step 1, sliding) The substrate slides onto Mia40, where it is oriented by the MISS/ITS through noncovalent, mainly hydrophobic interactions in the cleft of Mia40. The correct Cys of the substrate is thus primed to make the disulfide with Mia40. (step 2, docking) The substrate now docks onto Mia40 via the covalent mixed disulfide bond between the substrate-docking Cys and the juxtaposed active site Cys of Mia40. Finally, complete oxidation releases the substrate in a folded state. IM, inner membrane.

Materials and methods

Isolation of mitochondria

Wild-type mitochondria and *Mia40*-depleted mitochondria were isolated from the *S. cerevisiae* strain D273-10B (MAT-α) and from the *GAL-Mia40* strain as described previously (Daum et al., 1982; Glick, 1991; Banci et al., 2009) The yeast strains were grown at 30°C in medium containing 1% (wt/vol) yeast extract, 2% (wt/vol) bacto-peptone, and 2% lactate (vol/vol) pH adjusted to 5.5 (YPL). In the case of the *GAL-Mia40* strain, 0.2% glucose was added to maintain the suppression of the endogenous gene.

Generation of mutant substrate proteins

Truncated versions of yeast Tim10, -9, and -12 were amplified by PCR and cloned into a pSP64 vector (Promega) downstream of the SP6 promoter for in vitro transcription/translation purposes. For the N-terminal deletions, a Met was added at position 1. To improve ^{35}S labeling, three methionines were added at the C terminus where necessary. The sequence encoding the first 85 aa of cyb2, which constitutes its IMS-targeting sequence (Glick et al., 1992; Beasley et al., 1993; Schwarz et al., 1993), was then cloned upstream of ΔN39Tim10, ΔN28Tim12, and ΔN39Tim12 in pSP64. The cyb2-targeting sequence was amplified from pSM4 (a gift from B. Glick, University of Chicago, Chicago, IL) by PCR using appropriate primers. For complementation in the yeast *GAL-Tim12* strain, the whole cyb2ΔN28Tim12 and cyb2ΔN39Tim12 cassette was subcloned from pSP64 into pRS316, which contains the promoter and terminator of yeast Tim12. ITS-ΔN23 (C28S) Sue fusion was generated by PCR using a primer that amplified the truncated segment of Sue containing a Cys to Ser substitution at position 28 and contained the 32–40-aa segment of yeast Tim10 as a 5′ overhang. The fusion protein ITS-DHFR was amplified by PCR using as template the vector pQE16-DHFR (QIAGEN). The primer at the 5′ end contained the 32–40-aa segment of yeast Tim10 as an overhang. The fusion protein DHFR-ITS was amplified by PCR using as template the vector pQE16-DHFR (QIAGEN) with a primer that contained at the 3′ end the 32–40-aa segment of yeast Tim10 as an overhang. The fusion proteins ITS-F33A-DHFR and DHFR-ITS-F33A were cloned as ITS-DHFR and DHFR-ITS, respectively, but the primer contained the 32–40-aa segment of yeast Tim10 with a Phe substitution to Ala at position 33, which refers to the amino acid residue of the wild-type yeast Tim10. All fusion inserts were cloned in pSP64 for in vitro transcription/translation purposes. Yeast Mia40 ΔN290 containing a double Cys to Ser substitution at the CPC catalytic center was cloned in pET22 (EMD) for bacterial periplasmic expression with a C-terminal His_6 tag by PCR from pGEX/yMia40SPS (Banci et al., 2009). Amino acid substitutions for *COX17*, yeast *Cox17*, and yeast *Tim10* were generated by PCR-based site-directed mutagenesis (QuikChange site-directed mutagenesis kit; Agilent Technologies) from pSP64-based plasmids containing the *COX17*, yeast *Cox17*, and yeast *Tim10* gene, respectively. Primer design and the PCR conditions were performed according to the manufacturer's guidelines. The mutations were verified by sequencing reactions.

Import in yeast mitochondria

^{35}S-labeled precursor proteins were synthesized using the TNT SP6-coupled transcription/translation kit (Promega). The radioactive material was imported in 50–100 µg of wild-type yeast mitochondria in the presence of 2 mM ATP and 2.5 mM NADH for the indicated time points at 30°C. Mitochondria were then resuspended in 1.2 M sorbitol and 20 mM Hepes, pH 7.4, followed by a treatment with 0.1 mg ml^{-1} proteinase K with or without 1% (vol/vol) Triton X-100 to remove unimported material. Finally, they were resuspended in Laemmli sample buffer with or without β-Me as indicated, analyzed by SDS-PAGE, and visualized by digital autoradiography (Molecular Dynamics).

BN analysis of imported precursor

After import of radioactive ^{35}S-labeled protein in wild-type mitochondria, the samples were solubilized in 0.16% *N*-dodecylmaltoside buffer (50 mM NaCl, 10% glycerol, 20 mM Hepes/KOH, pH 7.4, 2.5 mM $MgCl_2$, 1 mM EDTA, and 1 mM PMSF) for 30 min on ice. The solubilized material was separated by a 20-min centrifugation at 100,000 *g*, which was then loaded on 6–16% gradient BN electrophoresis gel (Schägger and von Jagow, 1991; Schägger et al., 1994). The radioactive material was detected by autoradiography. For antibody depletion, the solubilized material was incubated with antibodies against Mia40 for 20 min on ice and then with protein A–Sepharose beads (GE Healthcare) for 20 min on ice. The unbound material was separated by centrifugation at 2,500 *g* for 2 min before loading on the gradient BN gel.

Coimmunoprecipitation of imported precursor in mitochondria

After import of radioactive ^{35}S-labeled protein in wild-type mitochondria for 10 min at 30°C, the samples were treated with 0.1 mg ml^{-1} proteinase K to remove unimported material. Mitochondria were then resuspended in

lysis buffer (150 mM NaCl, 10 mM Tris, pH 7.4, 0.5% Triton X-100, and 1% SDS) and boiled for 5 min at 95°C. The sample was then diluted 20 times with immunoprecipitation buffer (150 mM NaCl, 10 mM Tris, pH 7.4, and 0.5% Triton X-100) and incubated with antibodies against Mia40 and protein A–Sepharose beads for 2 h at 4°C. The bound material on the beads was washed three times with immunoprecipitation buffer and then resuspended in Laemmli sample buffer. The immunoprecipitated material was analyzed under reducing and nonreducing SDS-PAGE and visualized by digital autoradiography.

Protein purification

Recombinant proteins were expressed in the *Escherichia coli* BL21(DE3) strain from pET22a (ΔN290Mia40SPS) or pGEX (wild type, ΔN30, and ΔN39 Tim10 as a GST fusion) constructs. Cells carrying the pET22ΔN290Mia40SPS plasmid were harvested after induction with 0.4 mM IPTG for 3 h at 37°C. Cells were then resuspended in buffer A (150 mM NaCl and 50 mM Tris HCl, pH 7.4) and sonicated for 5 min at 50% amplification. Samples were centrifuged for 30 min at 4°C and 21,000 *g*. Protein was purified from the soluble fraction. 15 mM imidazole was added and then loaded onto Ni–nitrilotriacetic acid (NTA) resin (QIAGEN) using 2.5 ml of resin per liter of culture. Ni-NTA resin was washed in buffer A + 50 mM imidazole. Then, the protein was eluted by buffer A + 300 mM imidazole. Eluted protein was further purified by anion exchange chromatography on a MonoQ HR 5/5 column (GE Healthcare). Cells carrying the pGEX constructs were harvested after induction with 0.4 mM IPTG overnight at 18°C. Cells were then resuspended in buffer A and sonicated for 5 min at 50% amplification. Samples were centrifuged for 30 min at 4°C and 21,000 *g*. The soluble fraction was incubated with 1 ml of swollen glutathione beads per liter of culture overnight or for 6 h at 4°C. Beads were washed with buffer A and then eluted with buffer A + 50 mM reduced glutathione. Then, 5 U/ml thrombin was added and left to cut the GST tag overnight or for 6 h at 0°C. The cleaved fussed protein was isolated from the GST tag by gel filtration with a Superdex75 column (GE Healthcare).

Ni-NTA beads pull-down assay

Purified recombinant ΔN290Mia40SPS was incubated with Ni-NTA beads (QIAGEN) for 20 min at 4°C. 1 µg of pure protein was used per 1 µl of beads. The beads were washed with binding buffer (150 mM NaCl, 50 mM Tris, pH 7.4, 15 mM imidazole, 0.1% BSA, and 0.01% Triton X-100). ^{35}S-labeled proteins were produced using the TNT SP6-coupled transcription/translation kit. After the reaction, the lysates were treated with saturated $(NH_4)_2SO_4$ solution for 20 min in ice and centrifuged for 20 min at 16,000 *g* to precipitate the ^{35}S-labeled protein and remove the globins of the lysates. After precipitation, the pellet was resuspended in denaturing buffer (8 M urea, 150 mM NaCl, 50 mM Tris HCl, pH 8.0, and 1 mM DTT) in a volume equal to the volume of the lysates before precipitation and incubated for 1 h at room temperature. The denatured ^{35}S-labeled proteins were incubated with Ni-NTA beads equilibrated in binding buffer with or without ΔN290Mia40SPS (5 µl of denatured protein, 20 µl of beads, and 175 µl of binding buffer) for 2 h at the indicated temperature. After incubation, the beads were collected by centrifugation and washed three times with 180 µl of binding buffer. The bound material was resuspended in Laemmli sample buffer, separated by SDS-PAGE, and visualized by autoradiography.

ITC

ITC was used to measure the association constant, enthalpy (ΔH), entropy (ΔS), and free energy (ΔG) changes of Tim10 variants binding to ΔN290Mia40SPS. At least two independent measurements of the reaction were made at 25°C. All experiments were performed on VP-ITC microcalorimetry (MicroCal). Protein samples were extensively dialyzed against 50 mM KPi, pH 7.4, for 12 h at 4°C. To ensure full reduction of the proteins, they were incubated for 1 h with 10 mM TCEP (Tris [2-carbxyethyl]phosphine) at 4°C and then dialyzed for 1 h with 50 mM KPi, pH 7.4, and 1 mM TCEP at 4°C to make sure that the proteins were in the same buffer conditions. Tim10, ΔN30, and ΔN39 were used at 0.025 mM, and ΔN290Mia40SPS was injected at 0.25 mM at 15-s intervals. The concentration of the proteins was determined spectrophotometrically using their respective extinction coefficients.

Helical wheel projection and HADDOCK

Helical wheel representations were made using the helical wheel viewer for α helices from the University of Virginia in Charlottesville (http://cti.itc.virginia.edu/~cmg/Demo/wheel/wheelApp.html). Structural models of the transient complex between human MIA40 and human TIM9 and between human MIA40 and human TIM10 were obtained with the HADDOCK program (Dominguez et al., 2003), combining mutagenesis analysis with in silico docking. Indeed, we constrained the modeling, taking account of the mutational analysis data for MIA40 (Banci et al., 2009) and for the Tims (reported in this study) as well as the experimental data that the N-terminal Cys of the Tims makes a disulfide pair with C55 of MIA40 (Milenkovic et al., 2007; Sideris and Tokatlidis, 2007). The structures of $MIA40_{2S\text{-}S}$ (PDB ID 2K3J) and fully reduced TIM9 and -10 were used as input. The fully reduced TIM9 and -10 structures were generated from the human TIM9–TIM10 complex structure (PDB ID 2BSK) by removing the two disulphide bridges from the fully oxidized TIM9 and -10 protomer structures and randomly opening the two α helices. The residues engaged in the MIA40 interaction for TIM9 and -10, obtained by site-directed mutagenesis combined with in vitro and in vivo assays using the almost identical yeast homologues, were Tyr21, Leu24, and Cys28 and Tyr22, Met25, and Cys29, respectively. Corresponding residues for MIA40 engaged in interaction were Cys55, Leu56, Met59, Phe72, Phe75, Phe91, and Met94, which were similarly obtained from site-directed mutagenesis combined with in vitro and in vivo assays (Banci et al., 2009). A disulphide bond between Cys28 for TIM9 or Cys29 for TIM10 and Cys55 of MIA40 was also imposed in docking calculations. Structural models of the complexes between yCox17 and yMia40 and between COX17 and MIA40 were obtained with the HADDOCK program after the same aforementioned procedure. The structures of human MIA40 (PDB ID 2K3J) and yeast Mia40 (PDB ID 2ZXT) were used as input in the human and yeast complexes, respectively. The residues engaged in the Mia40 interaction for COX17 and yCox17, obtained by site-directed mutagenesis combined with in vitro and in vivo assays (Banci et al., 2009; this study), were Leu48, Ile49, His52, and Cys45 and Phe50, Ile51, Tyr54, and Cys57, respectively. A disulphide bond between Cys45 for COX17 or Cys57 for yCox17 and Cys55 of MIA40 or Cys298 of yMia40, respectively, was also imposed in docking calculations.

Miscellaneous

Complementation in the yeast strain *GAL-Tim12* was performed as described previously (Lionaki et al., 2008). In brief, the *GAL-Tim12* strain was transformed with the pRS316 plasmid harboring the corresponding genes (fusion constructs cyb2ΔN28Tim12 and cyb2ΔN39Tim12) under the control of the endogenous Tim12 promoter. The transformed clones were grown in minimal medium containing 0.2% GAL and then shifted to 0.2% glucose for 36 h before the complementation test. The same dilution of cells was dropped on either SC or SG plates (minimal medium with 0.2% glucose or 0.2% GAL, respectively) and incubated at 30°C for 4 d. SDS-PAGE was performed according to standard procedures. For the separation of proteins below 15 kD, Tris-Tricine SDS-PAGE was applied (Allen et al., 2003). Quantification of radioactive bands was performed using the Image Quant software (Molecular Dynamics), and error bars were generated by quantification of at least three independent experiments. In some figures, nonrelevant gel lanes were excised by digital treatment. Western blots were performed on nitrocellulose membranes according to standard procedures.

Online supplemental material

Fig. S1 shows the interaction of COX17 and its Cys mutants with Mia40 in mitochondria. Fig. S2 shows the interaction of yeast Cox17 and its Cys mutants with Mia40 in mitochondria. Fig. S3 shows the import controls as a percentage of the translation mix used for import. Fig. S4 shows the theoretical modeling of the yeast Cox17 docking to the yeast Mia40 substrate–binding cleft using HADDOCK. Fig. S5 shows the localization of ITS fusion constructs in wild-type mitochondria. Table S1 lists the calculated parameters of the data-driven docking of substrates to Mia40. Table S2 shows the prediction of ITS in Mia40 substrates. Online supplemental material is available at http://www.jcb.org/cgi/content/full/jcb.200905134/DC1.

We thank S. Karamanou (Foundation for Research and Technology Hellas, Heraklion, Crete, Greece) for help with ITC, N. Pfanner and A. Chacinska (University of Freiburg, Freiburg im Breisgau, Germany) for sharing unpublished data, S. Makrogikas and P. Kritsiligkou for help with some mutants, and members of our group for discussions and comments.

This work was supported by funds from the Institute of Molecular Biology and Biotechnology, Foundation for Research and Technology Hellas, the University of Crete, and the European Social Fund and national resources (to K. Tokatlidis), the European Network of Research Infrastructures for Providing

Access and Technological Advancements in Bio-NMR (contract no. 026145 to I. Bertini and L. Banci), and SPINE II (contract no. LSHG-CT-2006-031220). D.P. Sideris and N. Petrakis were supported by a PENED grant.

Submitted: 25 May 2009
Accepted: 19 November 2009

References

Abe, Y., T. Shodai, T. Muto, K. Mihara, H. Torii, S. Nishikawa, T. Endo, and D. Kohda. 2000. Structural basis of presequence recognition by the mitochondrial protein import receptor Tom20. *Cell*. 100:551–560. doi:10.1016/S0092-8674(00)80691-1

Allen, S., H. Lu, D. Thornton, and K. Tokatlidis. 2003. Juxtaposition of the two distal CX3C motifs via intrachain disulfide bonding is essential for the folding of Tim10. *J. Biol. Chem.* 278:38505–38513. doi:10.1074/jbc.M306027200

Arnesano, F., E. Balatri, L. Banci, I. Bertini, and D.R. Winge. 2005. Folding studies of Cox17 reveal an important interplay of cysteine oxidation and copper binding. *Structure*. 13:713–722. doi:10.1016/j.str.2005.02.015

Baker, M.J., C.T. Webb, D.A. Stroud, C.S. Palmer, A.E. Frazier, B. Guiard, A. Chacinska, J.M. Gulbis, and M.T. Ryan. 2009. Structural and functional requirements for activity of the Tim9-Tim10 complex in mitochondrial protein import. *Mol. Biol. Cell*. 20:769–779. doi:10.1091/mbc.E08-09-0903

Banci, L., I. Bertini, S. Ciofi-Baffoni, A. Janicka, M. Martinelli, H. Kozlowski, and P. Palumaa. 2008. A structural-dynamical characterization of human Cox17. *J. Biol. Chem.* 283:7912–7920. doi:10.1074/jbc.M708016200

Banci, L., I. Bertini, C. Cefaro, S. Ciofi-Baffoni, A. Gallo, M. Martinelli, D.P. Sideris, N. Katrakili, and K. Tokatlidis. 2009. MIA40 is an oxidoreductase that catalyzes oxidative protein folding in mitochondria. *Nat. Struct. Mol. Biol.* 16:198–206. doi:10.1038/nsmb.1553

Beasley, E.M., S. Müller, and G. Schatz. 1993. The signal that sorts yeast cytochrome b2 to the mitochondrial intermembrane space contains three distinct functional regions. *EMBO J.* 12:2303–2311.

Chacinska, A., S. Pfannschmidt, N. Wiedemann, V. Kozjak, L.K. Sanjuán Szklarz, A. Schulze-Specking, K.N. Truscott, B. Guiard, C. Meisinger, and N. Pfanner. 2004. Essential role of Mia40 in import and assembly of mitochondrial intermembrane space proteins. *EMBO J.* 23:3735–3746. doi:10.1038/sj.emboj.7600389

Daum, G., P.C. Böhni, and G. Schatz. 1982. Import of proteins into mitochondria. Cytochrome b2 and cytochrome c peroxidase are located in the intermembrane space of yeast mitochondria. *J. Biol. Chem.* 257:13028–13033.

Diekert, K., G. Kispal, B. Guiard, and R. Lill. 1999. An internal targeting signal directing proteins into the mitochondrial intermembrane space. *Proc. Natl. Acad. Sci. USA*. 96:11752–11757. doi:10.1073/pnas.96.21.11752

Dominguez, C., R. Boelens, and A.M. Bonvin. 2003. HADDOCK: a protein-protein docking approach based on biochemical or biophysical information. *J. Am. Chem. Soc.* 125:1731–1737. doi:10.1021/ja026939x

Everard-Gigot, V., C.D. Dunn, B.M. Dolan, S. Brunner, R.E. Jensen, and R.A. Stuart. 2005. Functional analysis of subunit e of the F1Fo-ATP synthase of the yeast *Saccharomyces cerevisiae*: importance of the N-terminal membrane anchor region. *Eukaryot. Cell*. 4:346–355. doi:10.1128/EC.4.2.346-355.2005

Gabriel, K., D. Milenkovic, A. Chacinska, J. Müller, B. Guiard, N. Pfanner, and C. Meisinger. 2007. Novel mitochondrial intermembrane space proteins as substrates of the MIA import pathway. *J. Mol. Biol.* 365:612–620. doi:10.1016/j.jmb.2006.10.038

Glick, B.S. 1991. Protein import into isolated yeast mitochondria. *Methods Cell Biol.* 34:389–399. doi:10.1016/S0091-679X(08)61693-3

Glick, B.S., A. Brandt, K. Cunningham, S. Müller, R.L. Hallberg, and G. Schatz. 1992. Cytochromes c1 and b2 are sorted to the intermembrane space of yeast mitochondria by a stop-transfer mechanism. *Cell*. 69:809–822. doi:10.1016/0092-8674(92)90292-K

Heaton, D., T. Nittis, C. Srinivasan, and D.R. Winge. 2000. Mutational analysis of the mitochondrial copper metallochaperone Cox17. *J. Biol. Chem.* 275:37582–37587. doi:10.1074/jbc.M006639200

Hell, K. 2008. The Erv1-Mia40 disulfide relay system in the intermembrane space of mitochondria. *Biochim. Biophys. Acta*. 1783:601–609. doi:10.1016/j.bbamcr.2007.12.005

Lionaki, E., C. de Marcos Lousa, C. Baud, M. Vougioukalaki, G. Panayotou, and K. Tokatlidis. 2008. The essential function of Tim12 in vivo is ensured by the assembly interactions of its C-terminal domain. *J. Biol. Chem.* 283:15747–15753. doi:10.1074/jbc.M800350200

Lu, H., S. Allen, L. Wardleworth, P. Savory, and K. Tokatlidis. 2004. Functional TIM10 chaperone assembly is redox-regulated in vivo. *J. Biol. Chem.* 279:18952–18958. doi:10.1074/jbc.M313045200

Mesecke, N., N. Terziyska, C. Kozany, F. Baumann, W. Neupert, K. Hell, and J.M. Herrmann. 2005. A disulfide relay system in the intermembrane space of mitochondria that mediates protein import. *Cell*. 121:1059–1069. doi:10.1016/j.cell.2005.04.011

Milenkovic, D., K. Gabriel, B. Guiard, A. Schulze-Specking, N. Pfanner, and A. Chacinska. 2007. Biogenesis of the essential Tim9-Tim10 chaperone complex of mitochondria: site-specific recognition of cysteine residues by the intermembrane space receptor Mia40. *J. Biol. Chem.* 282:22472–22480. doi:10.1074/jbc.M703294200

Milenkovic, D., T. Ramming, J.M. Müller, L.S. Wenz, N. Gebert, A. Schulze-Specking, D. Stojanovski, S. Rospert, and A. Chacinska. 2009. Identification of the signal directing Tim9 and Tim10 into the intermembrane space of mitochondria. *Mol. Biol. Cell*. 20:2530–2539. doi:10.1091/mbc.E08-11-1108

Müller, J.M., D. Milenkovic, B. Guiard, N. Pfanner, and A. Chacinska. 2008. Precursor oxidation by Mia40 and Erv1 promotes vectorial transport of proteins into the mitochondrial intermembrane space. *Mol. Biol. Cell*. 19:226–236. doi:10.1091/mbc.E07-08-0814

Naoé, M., Y. Ohwa, D. Ishikawa, C. Ohshima, S. Nishikawa, H. Yamamoto, and T. Endo. 2004. Identification of Tim40 that mediates protein sorting to the mitochondrial intermembrane space. *J. Biol. Chem.* 279:47815–47821. doi:10.1074/jbc.M410272200

Reddehase, S., B. Grumbt, W. Neupert, and K. Hell. 2009. The disulfide relay system of mitochondria is required for the biogenesis of mitochondrial Ccs1 and Sod1. *J. Mol. Biol.* 385:331–338. doi:10.1016/j.jmb.2008.10.088

Rissler, M., N. Wiedemann, S. Pfannschmidt, K. Gabriel, B. Guiard, N. Pfanner, and A. Chacinska. 2005. The essential mitochondrial protein Erv1 cooperates with Mia40 in biogenesis of intermembrane space proteins. *J. Mol. Biol.* 353:485–492. doi:10.1016/j.jmb.2005.08.051

Schägger, H., and G. von Jagow. 1991. Blue native electrophoresis for isolation of membrane protein complexes in enzymatically active form. *Anal. Biochem.* 199:223–231. doi:10.1016/0003-2697(91)90094-A

Schägger, H., W.A. Cramer, and G. von Jagow. 1994. Analysis of molecular masses and oligomeric states of protein complexes by blue native electrophoresis and isolation of membrane protein complexes by two-dimensional native electrophoresis. *Anal. Biochem.* 217:220–230. doi:10.1006/abio.1994.1112

Schwarz, E., T. Seytter, B. Guiard, and W. Neupert. 1993. Targeting of cytochrome b2 into the mitochondrial intermembrane space: specific recognition of the sorting signal. *EMBO J.* 12:2295–2302.

Sideris, D.P., and K. Tokatlidis. 2007. Oxidative folding of small Tims is mediated by site-specific docking onto Mia40 in the mitochondrial intermembrane space. *Mol. Microbiol.* 65:1360–1373. doi:10.1111/j.1365-2958.2007.05880.x

Terziyska, N., T. Lutz, C. Kozany, D. Mokranjac, N. Mesecke, W. Neupert, J.M. Herrmann, and K. Hell. 2005. Mia40, a novel factor for protein import into the intermembrane space of mitochondria is able to bind metal ions. *FEBS Lett.* 579:179–184. doi:10.1016/j.febslet.2004.11.072

Terziyska, N., B. Grumbt, M. Bien, W. Neupert, J.M. Herrmann, and K. Hell. 2007. The sulfhydryl oxidase Erv1 is a substrate of the Mia40-dependent protein translocation pathway. *FEBS Lett.* 581:1098–1102. doi:10.1016/j.febslet.2007.02.014

Terziyska, N., B. Grumbt, C. Kozany, and K. Hell. 2009. Structural and functional roles of the conserved cysteine residues of the redox-regulated import receptor Mia40 in the intermembrane space of mitochondria. *J. Biol. Chem.* 284:1353–1363. doi:10.1074/jbc.M805035200

Tokatlidis, K., T. Junne, S. Moes, G. Schatz, B.S. Glick, and N. Kronidou. 1996. Translocation arrest of an intramitochondrial sorting signal next to Tim11 at the inner-membrane import site. *Nature*. 384:585–588. doi:10.1038/384585a0

Webb, C.T., M.A. Gorman, M. Lazarou, M.T. Ryan, and J.M. Gulbis. 2006. Crystal structure of the mitochondrial chaperone TIM9.10 reveals a six-bladed alpha-propeller. *Mol. Cell*. 21:123–133. doi:10.1016/j.molcel.2005.11.010